Journal of Volcanology and Geothermal Research 202 (2011) 96–106

Contents lists available at ScienceDirect

Journal of Volcanology and Geothermal Research

journal homepage: www.elsevier.com/locate/jvolgeores

Structures and evolution of the plumbing system of Piton de la Fournaise volcano inferred from clustering of 2007 eruptive cycle seismicity ☆

Frédérick Massin [a,b,*], Valérie Ferrazzini [b], Patrick Bachèlery [a], Alexandre Nercessian [c], Zacharie Duputel [d], Thomas Staudacher [b]

[a] Laboratoire GéoSciences Réunion, Université de La Réunion, UMR CNRS 7154 IPGP, 15 Avenue René Cassin, 97715 Saint-Denis cedex 9, La Réunion, France
[b] Observatoire Volcanologique du Piton de la Fournaise, Institut de Physique du Globe de Paris, UMR CNRS 7154 IPGP, 14 RN3 - Km 27, 97418 La Plaine des Cafres, La Réunion, France
[c] Laboratoire de Sismologie, Institut de Physique du Globe de Paris, Boite 89, 4 place Jussieu, 75252 Paris cedex 05, France
[d] Institut de Physique du Globe de Strasbourg, IPGS - UMR 7516, CNRS and Université de Strasbourg (EOST), France

ARTICLE INFO

Article history:
Received 28 June 2010
Accepted 30 January 2011
Available online 5 March 2011

Keywords:
Piton de la Fournaise
caldera
CLVD
sill
volcano monitoring
volcano-tectonic earthquakes
clustering
earthquake relocation
composite focal mechanism

ABSTRACT

Analysis of seismic activity associated with the eruptions of 2007, which led to the collapse of the Dolomieu crater on April 5th, reveals the link between the seismicity and the magma transfers at Piton de la Fournaise. Three eruptive phases occurred on February 18th, March 30th and April 2nd, 2007, at the summit, 2,000 m, and 600 m high on the South-East flank respectively, illustrating the three types of eruptions defined for the current Piton de la Fournaise activity. We use cross-correlation of seismic waveforms and clustering to improve the earthquake locations and determine the best-constrained focal mechanisms (with an average of 78 P phase polarities). The pre-eruptive seismicity of the February and March eruptions is composed of time extended clusters that also preceded other distal eruptions from 2000 to 2007. Our analysis shows that the seismic swarm prior to the February eruption initiated the intrusion that led to the April 2007 eruption. The seismicity preceding the Dolomieu crater collapse consists of numerous, but time-limited, clusters and specific seismic activity that accompanied the Dolomieu crater collapse. From April 1st to April 5th, earthquakes with CLVD mechanisms combined with normal faulting sources occurred between 0.8 and 0 km asl, until the complete rupture of the shallow magma storage roof. This collapse induced the propagation of a de-pressurization front and triggered a migration of seismicity from 0 to −8 km along a very narrow path.

1. Introduction

Caldera collapses due to lateral eruptions are typical of basaltic volcanoes and some historical examples are well-documented, including for the 1924 eruption at Kilauea, Hawaii (Dvorak, 1992), the 1968 eruption at Fernandina, Galapagos (Simkin and Howard, 1970), the 1975–1977 eruption at Tolbachik, Kamchatcka (Fedotov et al., 1980) and the 2000 eruption at Miyakejima volcano, Japan (Geshi et al., 2002). On the other hand, caldera formation may also occur in subduction zones. Hildreth and Fierstein (2000) described the summit collapse that occurred during the 1912 lateral eruption on the Katmai volcano. They notice that the seismic activity associated with the collapse released 250 times more seismic energy than the 1991 Pinatubo eruption and caldera collapse (Philippines) that could be due to the absence of a pre-existing caldera fault at Mount Katmai. Smaller collapse structures are also present at Piton de la Fournaise such as the 1986 collapse of an 80 m pit-crater at the end of the 1985–1986 eruptive cycle (Lenat et al., 1989). Hirn et al. (1991) report dilatation compensated linear vector dipoles (D-CLVD) prior to the pit-crater formation. They interpreted these events as a sudden increase of fluid volume in vertical fluid filled cracks linked to underlying magma storage (Aki, 1984; Julian and Sipkin, 1985; Chouet and Julian, 1985; Kanamori et al., 1993). Hirn et al. (1991) also observed long-period seismic events during the subsidence of the pit-crater presenting similar features with the seismic events associated with the Fernandina caldera collapse described by Filson et al. (1973). Both authors considered these events as the excitation of the resonance of empty cavities resulting from magma withdrawal. At the Miyakejima volcano, Uhira et al. (2005) relocated the hypocenters of the pre-collapse lateral migration and determined strike-slip and oblique focal mechanisms. Kikuchi et al. (2001) studied the syn-collapse seismicity and observed a very-long-period seismic swarm under the summit. Kumagai et al. (2001) performed an inversion of the syn-collapse seismicity and proposed a model in which a vertical piston of solid materials in the conduit is intermittently forced into the magma chamber by lateral magma outflow. Independently, Geshi et al. (2002) detailed the caldera structure and the nature of the eruptive materials and suggested that

☆ Clustering of Piton de la Fournaise seismicity.

* Corresponding author at: Laboratoire GéoSciences Réunion, Université de La Réunion, UMR CNRS 7154 IPGP, 15 Avenue René Cassin, 97715 Saint-Denis cedex 9, La Réunion, France. Tel.: +33 801 581 7856; fax: +33 801 581 7065.
URL: http://sites.google.com/site/fredmassin/ (F. Massin).

0377-0273/$ – see front matter © 2011 Elsevier B.V. All rights reserved.
doi:10.1016/j.jvolgeores.2011.01.008

subsidence was caused by the upward migration of a steam-filled cavity. The results of seismic studies of caldera collapses all suggest the crushing of magma storage zones. However, structural studies are hardly compatible with the seismic models. Most seismic studies focus on the syn-collapse seismic events and studies of the birth, the development, and the evolution of collapsing structures have not been performed.

Here we study the 2007 eruptions of Piton de la Fournaise volcano, La Réunion (France), and the April 2007 collapse using the seismic data of the Piton de la Fournaise Volcano Observatory (OVPF). The main objective of our study is to characterize the structures, their origins and the mechanism of the summit collapse of Piton de la Fournaise (PdF). In order to propose a comprehensive view of the seismicity, we use a waveform cross-correlation technique to define the pre-existing and newborn seismic structures. Waveform similarity is used here as a tool to recognize the activation of each seismogenic structure without being disturbed by the hypocenter uncertainties of low magnitude earthquakes. Battaglia et al. (2005) already used cross-correlation at PdF for absolute location. Since Fremont and Malone (1987), cross-correlation has also shown great success in various tectonic environments including volcanoes (Got et al., 1994; Waldhauser and Ellsworth, 2000; Rowe et al., 2004; Clarke et al., 2009). The automated correlation and clustering methods reduce picking inconsistencies and improve the earthquake locations for determining the best-constrained focal mechanisms. Relocation and determination results are then used for co-seismic slip extraction and stress field study.

2. Volcanological settings and chronology

PdF, which originates from the La Réunion hotspot, is one of the world's most active basaltic shield volcanoes (Courtillot et al., 1986; Lénat and Bachèlery, 1990). Its activity is mostly concentrated at the top of the 400 m high cone that formed within the 4.5 ky-old Enclos Fouqué caldera (Fig. 1; Bachèlery, 1981). Eruptions occur less frequently outside the caldera along the NE and SE rift zones. The last of these was the 1986 eruption, during which the summit experienced a pit-crater collapse (Lenat et al., 1989; Hirn et al., 1991). Considering the location of the eruptive sites, three different types of eruptions have been defined (Peltier et al., 2008) (i) summit eruptions start and remain in the summit collapsed structure; (ii) proximal eruptions begin at or close to the summit and subsequently propagate downhill; (iii) distal eruptions arise on the volcano flank, several kilometers away from the summit. The occurrence of coalescent collapse structures at the summit of the active cone suggests that the eruptive activity was contemporaneous with recurrent collapse events (Lénat and Bachèlery, 1990; Carter et al., 2007). The two most recent structures correspond to Bory and Dolomieu craters (Fig. 1).

In 1998, the eruptive activity at PdF resumed after a 6 year lull. Since then, the volcano experienced two successive eruptive patterns, which show differences in terms of seismicity and deformation of the edifice (Michon et al., 2007; Peltier et al., 2009). Before 2000, eruptions were preceded by a few days of low-level seismicity. Once the eruption started, volcano-tectonic (VT) events seldom occurred and the tremor progressively decreased until it disappeared. Since 2000, the volcano underwent significant pre-eruptive inflation accompanied by increasing seismic activity. Earthquake occurrence that usually stops at the onset of an eruptive phase resume to a high rate accompanied by an increased eruptive tremor amplitude and eventually both stopped within a minute of each other. This latter phase was particularly important during distal eruptions (Michon et al., 2007). Since 2000, the eruptive activity was also characterized by the occurrence of eruptive cycles starting with summit eruptions and ending with distal ones (Peltier et al., 2008a). Recently, Peltier et al. (2009) suggest that the August 2006 summit eruption was the beginning of the 2006–2007 eruptive cycle of PdF volcano.

Three eruptive phases occurred in 2007, illustrating the three types of the current PdF eruptions (see Table 1 and Peltier et al., 2009). On February 18th a summit eruption, preceded by a 27 minute-long seismic swarm located above sea level, under the summit of PdF, took place along an east–west fissure across the Dolomieu crater and lasted

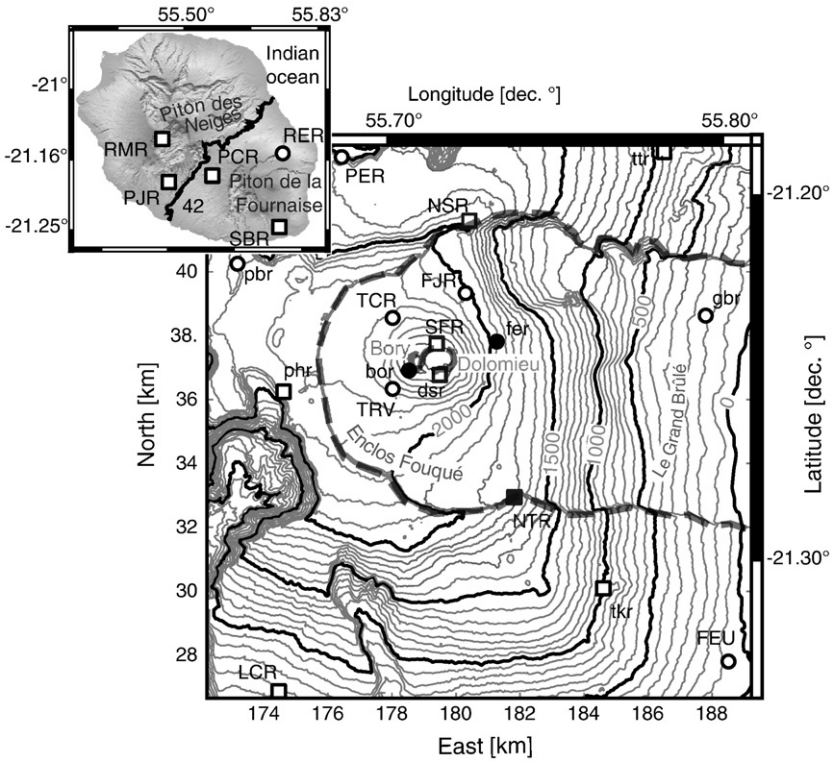

Fig. 1. Sketch map of the PdF seismic array in the eastern part of La Réunion, Indian ocean, with the seismometers of the OVPF. Circles : three components seismometers ; squares : vertical seismometers. Seismometers used for cross correlation are indicated with black filled symbols.

Table 1
Eruptions of PdF volcano during the 2007 year.

Date	Seismic-crisis duration [min]	Fissure altitude [m]	Tremor duration	Type
February 18th, 2007	27	2500	9 h	Summit
March 30th, 2007	144	1880	10 h	Proximal
April 2nd, 2007	2940	575	27 d	Distal

9 h. The next eruption occurred on March 30th after a seismic swarm of 144 min. The VT earthquake's foci of the seismic crisis first shifted towards the north-east part of the Enclos Fouqué and then towards the south-east. This eruption was a proximal eruption, at an elevation of 1900 m, on the south-east flank of the central cone and lasted 10 h. Between March 31st and April 2nd, a seismic swarm occurred, with several thousands of VT earthquakes under the summit and under the eastern slope of PdF. On April 2nd, at 6:00, a 27 day-long distal eruption started on the south-east rift-zone of PdF, 8 km away from the summit, at an altitude of about 600 m in the Enclos Fouqué. Dolomieu crater collapsed on April 5th and 6th, during a paroxysmal phase of activity. The collapse came with cycles of increasing seismic noise. The first of them ended with a Md 3.2 earthquake (the 5th April, at 20:48, Staudacher et al., 2009). Michon et al. (2007) and Staudacher et al. (2009) described these cycles and showed the link between the cycles of seismic noise, ground deformation, and the tremor step-by-step amplification at the locus of the eruption. They observed that the cycles corresponded to the Dolomieu crater collapse in a fast succession of subsidence events. The April 2nd, 2007 eruption of the PdF volcano produced 180×10^6 m^3 of lava which is the largest volume known for the historical period, with half of the volume erupted on land (Staudacher et al., 2009) and half in the ocean (Saint-Ange, 2009). As a result of this eruption, the Dolomieu crater collapsed to form a depression with a depth of 330 m and a volume of about 110×10^6 m^3 (Urai et al., 2007; Staudacher et al., 2009). This pit-crater formation was one of the best instrumented since the Miyakejima summit crater collapse in 2000 (Geshi et al., 2002; Michon et al., 2007).

3. Data acquisition and selection

The OVPF seismological network is composed of 25 seismometers. Vertical and 3-component seismometers are indicated in Fig. 1. The seismic stations are installed in concentric circles around the summit of the volcano. Data are transmitted by radio to the observatory and continuously recorded and analyzed using the *Earthworm* data acquisition program (Johnson, 1995). From January 2007 to the end of October 2007, we recorded over 4250 triggers, 714 of which have been manually located using an average of 12 picked phases per event. The *Earthworm* module is set to detect the smallest events and a first task was to eliminate all spurious events such as thunder, rock falls, or helicopters triggers. In order to do so, we computed the cross-correlation coefficient of the 714 located events with the set of 4250 triggered events using the vertical component of the station *bor* (Fig. 1). This station is best situated to record the smallest events. We then selected all the events that gave a cross-correlation coefficient greater than 0.5 and recovered a set of 1866 events that added to our first selection, which forms the starting dataset of our study. This task was performed using short signal windows of five seconds that, at the scale of the volcano, include P and S phases.

4. Data processing

4.1. Clustering

We developed an automatic cross-correlation and clustering algorithm with Matlab for measuring waveform similarity. The first task is to compute the cross-correlation coefficient between all possible pairs of events on the vertical component of a given station. We used unfiltered waveforms of 17 s long of all the formerly selected events. In order to avoid missing small events, this task has been completed for three stations. The first station is *bor*, which has the best signal to noise ratio on the main part of the seismicity. The second station is *fer*, which is the station with the best signal to noise ratio located on the east side of PdF. The third, *NTR*, is a station located on the southern cliff of the Enclos Fouqué caldera, close to the April eruption area. Two pairs of events, A–B and C–B, were merged into one cluster if they involved a common event, B, and if they reached the cross-correlation coefficient threshold of 0.85 on one of the three stations. A visual checkout was required to remove glitch-type clusters. Using this technique, 443 clusters were selected to form the cluster dataset containing 1625 repeating events. In each cluster, we chose a master, which has the best-constrained absolute locations. The masters have at least 12 picked P- and S-wave phases, including an average of three S-wave phases (one S-wave phase at least). Considering each cluster, the pick times of the master earthquake were applied to each slave event using the alignment of waveforms at the maximum of the cross-correlation function (Fig. 2, clusters A, B and C). Using these pick times, we computed the absolute locations of the best 1052 clustered earthquakes from a modified version of *hypo71* (Lee and Lahr, 1975) by Nercessian et al. (1996) that takes into account the travel time along the ray to correct for the station elevation. The input velocity ratio is the same as in other studies on PdF (Hirn et al., 1991; Nercessian et al., 1996; Battaglia et al., 2005). Results from the 1052 locations show an median horizontal and vertical error of 250 ± 3040 m and 300 ± 1800 km respectively with a RMS of 0.09 ± 0.46 s. For the master locations, these errors reduce to 185 ± 470 m, 300 ± 720 m and 0.09 ± 0.018 s respectively. The distribution of the repeating earthquakes around their respective cluster centroids is depicted by the histograms in Figs. 3A and 4A.

4.2. Relative relocation and source determination

Because of the low magnitude of the seismicity of PdF, it is preferable to set the relative positions of clustered earthquakes from the absolute position of their respective master earthquakes. The clusters were used to produce a cross-correlation catalog for *hypoDD*, that contains, for each clustered event, the differential travel times between the event and its master for each picked phase (Waldhauser and Ellsworth, 2000). The set of clusters has been relocated using *hypoDD* (Waldhauser and Ellsworth, 2000). Following Waldhauser and Ellsworth (2000), our cross-correlation catalog minimizes the number of earthquake pairs. *HypoDD* uses differential travel time from both travel time similarities and waveform cross-correlation similarities. Using both catalogs allow to form and solve the double-difference equation systems at the scale of the whole seismicity and at the scale of the waveform cluster. The chosen LSQR mode (Paige and Saunders, 1982) can efficiently solve a large system of equations but the errors reported are underestimated and poorly constrained (Waldhauser and Ellsworth, 2000). All the relocated earthquakes have more than eight travel time similarities and four cross-correlated travel time similarities. The *hypoDD* input consisted of 274,562 P and 45,072 S travel time differences from travel time similarities and 35,476 P and 4,079 S travel time differences from cross-correlation. Using this approach, 633 out of 1052 earthquakes were relocated that precisely overlapped the 461 earthquakes relocated in the SVD mode. LSQR results are used in our study. The 633 LSQR relocated earthquakes have a median horizontal relative error of 73 ± 65 m, a median vertical relative error of 97 ± 80 m, a median RMS of 0.008 ± 0.048 s on the travel time similarities catalog and of 0.018 ± 0.012 s on the cross-correlated similarities catalog. The horizontal and vertical errors reported in the SVD mode are 55 ± 422 m and 52 ± 280 m. The 633 relocated earthquakes made up a dataset of 292 relocated clusters. The proportion of located and relocated earthquakes of each

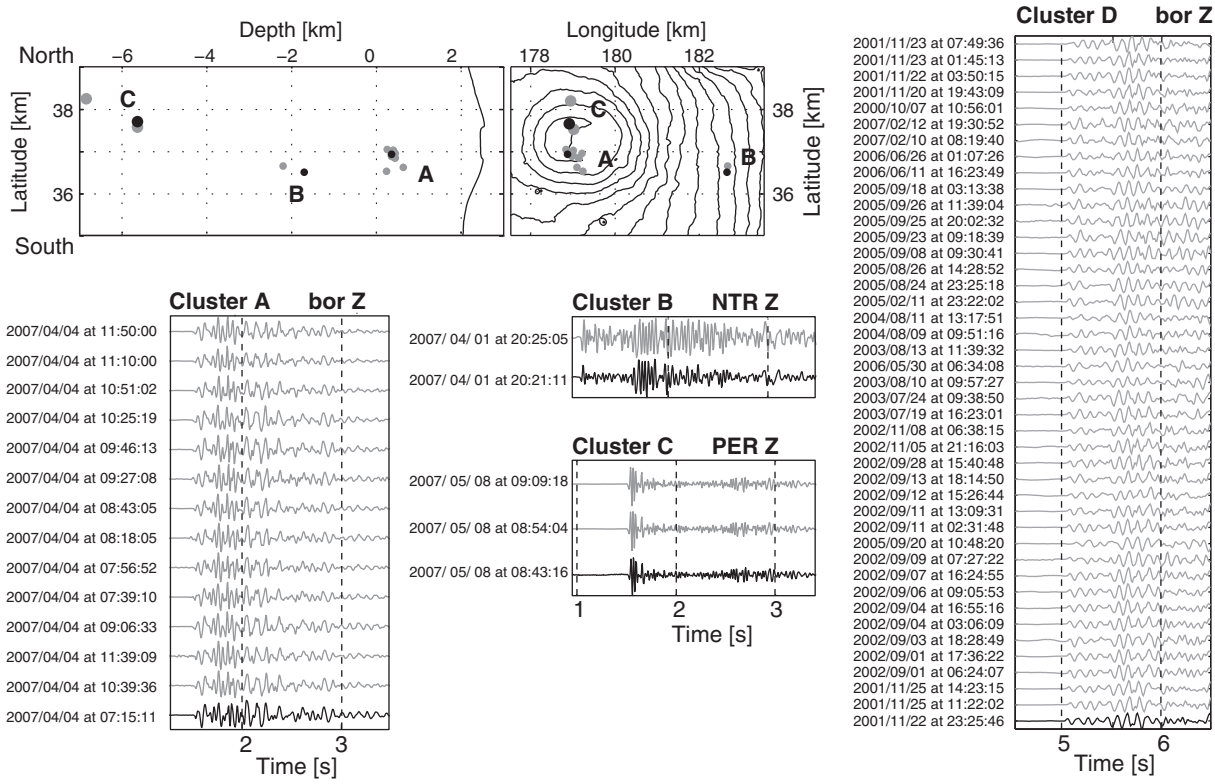

Fig. 2. Comparison between locations and waveforms. Three clusters are represented, A : around sea level, B : under east side of PdF, and C : at −5 km above sea level. For each cluster, the black earthquake (black dot on map and black waveform) is the hand localized master (best constrained location), the gray earthquakes represent the hand localized slaves (their corrected pick times are aligned on the master). Cluster D is extract from Massin (2009) and regroup repeating earthquakes from 2000 to 2007.

clusters is represented by histograms on the right side of Fig. 3A. The improvement in clustered earthquakes distribution in each cluster is represented in the right histogram of Fig. 3A. To perform the source determinations, we extracted only the 230 clusters having more than three earthquakes. Composite focal mechanisms were determined using *FPFIT* (Reasenberg and Oppenheimer, 1985) for each cluster considering a set of 78 P phase polarities on average. The position of each composite focal mechanism is set at the master hypocenter.

5. Results

5.1. Correlation highlights earthquake organization

Fig. 3A displays the cluster activation as a function of time for the year 2007. Clusters are classified in six types depending on their lifetime. The first group of dark clusters occurred only in the pre-eruptive period of February. Another group of magenta clusters occurred only during the March pre-eruptive period. Related to these two periods, transition clusters represent earthquakes that preceded both February 18th and March 30th eruptions. The red clusters are associated with the pre-eruptive activity of the April eruption (from March 31st to April 2nd) and with pre-collapse seismicity. The latter contain (in red) the largest number of clusters that also includes the largest number of events. Between April 2nd and the collapse, the lifetime of these clusters is limited to a few days. After the collapse, the cluster lifetime tends to increase until the end of eruption. Fig. 3B displays the cluster activation as a function of time for the 2000–2008 time period from Massin (2009). The pre-eruptive seismicity of the April distal eruption reactivated several clusters that can be found preceding other distal eruptions of the 2000–2008 time period. Fig. 3B suggests that the structures involved during the pre-eruptive seismic swarm of February, March, and April correspond to main structures that were reactivated since June 2000. On the other hand, the seismic swarm prior to the Dolomieu crater collapse is composed by numerous and large clusters that have a very short lifetime of about 5 days. The growing of main structures and their seismicity has been observed since June 2000 to March 31st 2007, but the Dolomieu collapse was associated with new-born seismic sources from April 2nd and April 5th 2007.

Fig. 4A and B display maps and cross sections of earthquake locations. The histograms of Fig. 4 allow the direct estimation of the relocation effect on repeating earthquake distribution. The general decay of the total number of earthquakes after relocation should consider to estimate the relocation effect. In location results, clustered earthquakes have a median distance to centroids of 0.32 ± 1.45 km. The relocation improves the median distance to 100 ± 220 m. Overall, in Fig. 4B, hypocenters show smaller spatial dispersion than in Fig. 4A. Fig. 4B also shows narrower seismic zones and highlights four levels of seismicity. Superficial seismicity occurs above 0.8 km asl (above sea level). The densest located seismicity takes place between 0.8 km and sea level and most of the earthquakes during pre-eruptive periods and seismic swarms occur in this level which also involves the largest magnitude earthquakes. A third level between 0 and −0.5 km is less active (active only during and after April). The deeper level on Fig. 7E extends vertically from −3 km to −8 km, with a denser stage between −4.5 km and −5 km. Other seismic clusters have been relocated under the eastern flank of le PdF around −2 km, making up a fifth isolated level.

5.2. Source mechanisms analysis

The source mechanisms of 154 clusters have been identified as pure double-couple mechanisms. Most of the double couple solutions correspond to earthquakes occurring between February and March 2007. Strike, dip and rake have average uncertainties of 4.8°, 4.0° and 6.6° respectively. Since we do not consider the heterogeneity of elastic properties in the description of the results, we shall consider the relative position of clusters rather than the absolute location of each source.

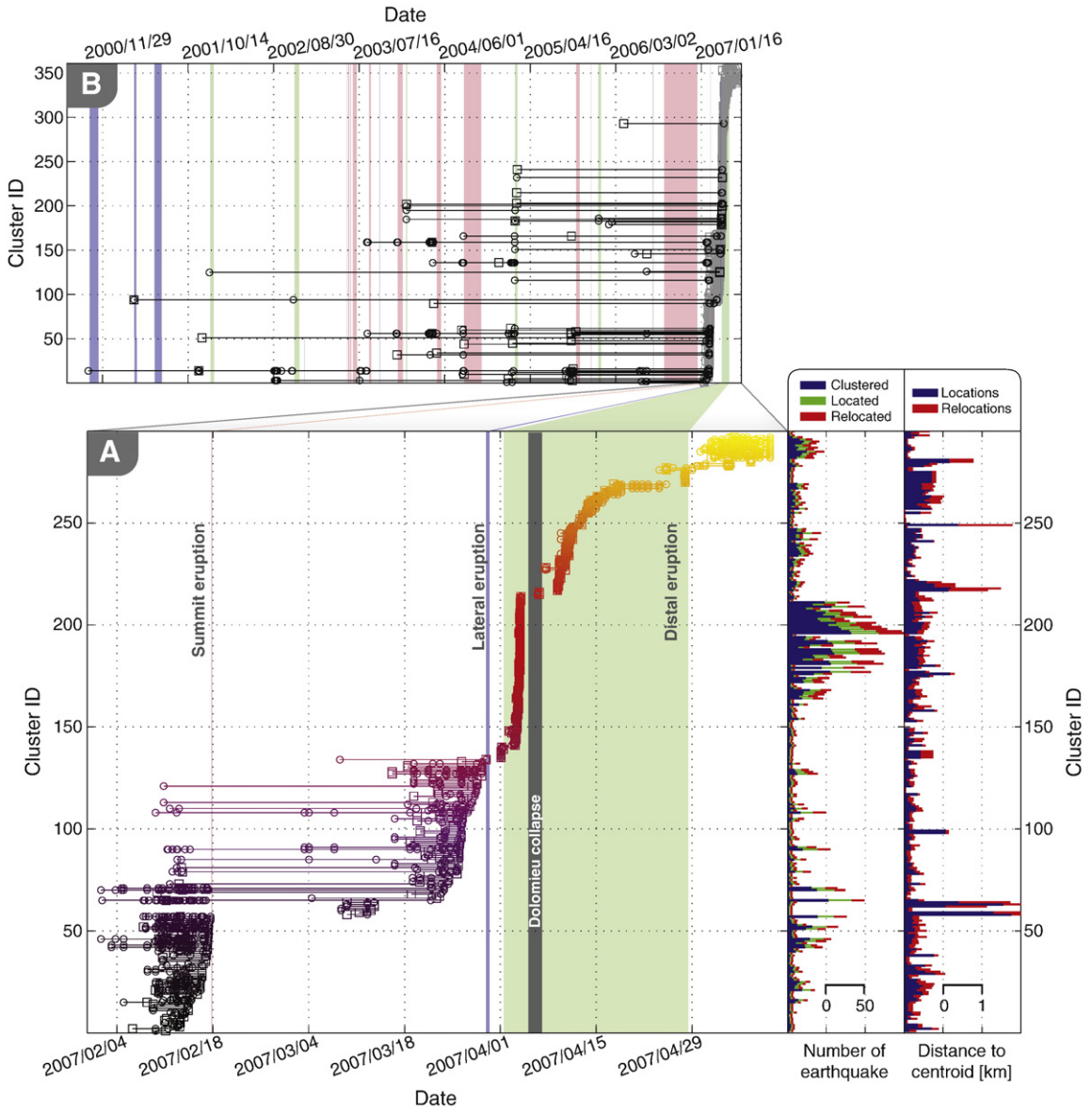

Fig. 3. Representation of cross-correlation clusters. Earthquakes belonging to the same cluster are on the same line. Each circle is an earthquake placed along the X axis as a function of origin time. A circle depicts each event along a line that represents the cluster to which the event belongs. The master earthquake of each family is represented by a square on the line. A: clusters associated to the 2007 eruptions. Left histogram : numbers of clustered, located and relocated earthquakes by cluster. Right histogram : average distances from cluster centroid to clustered earthquakes, locations and relocations are both represented. B: clusters associated with the 2007 eruption and the other eruptions of the 2000–2007 time period from Massin (2009), see Fig. 2D for waveforms examples.

Examples of source mechanisms are shown in Fig. 5. We identified pure double couple sources, oriented as strike slip (Fig. 5A) and normal fault, but also non-double couple (non-DC) clusters with either an isolated phase of compression (Fig. 5B) or dilatation (Fig. 5C) on *bor* and *dsr* stations. Very similar non-DC seismicity has already been observed by Hirn et al. (1991), associated with the March 1986 pit-crater collapse at PdF. Following Hirn et al. (1991), we hypothesized this non-DC cluster as Compensated Linear Vector Dipole clusters (CLVD, Knopoff and Randall, 1970) on the basis of first motions polarities. We assume that only the 76 clusters with identical first motion polarities on all clustered events could respect this hypothesis. These clusters are hypothesized as dilatation CLVD (D-CLVD) when they show a vertical dilatation axis (14 clusters as in Fig. 5B) and vertical compression clusters are hypothesized as compression CLVD (62 C-CLVD clusters, as in Fig. 5C).

Figs. 6 and 7 show the focal mechanism solutions with colors according to the clusters. Clusters are depicted as a function of time on the right side. Fig. 6A shows the transition clusters of Fig. 3A activated before the February and March eruptions. From these 26 clusters, 4 clusters are not interpretable, 5 clusters have been identified as D-CLVD, 6 clusters have been determined as strike-slip faulting events, 9 clusters have been determined as normal faulting events and 2 have been determined as reverse faults. Hypocenters are distributed along two branches from 0.3 to 0.8 km (asl), under the northern and the southern part of the summit. Between 0.3 and 0.8 km asl, the northern branch is the site of a well aligned normal fault that underlines the northern scarp of Bory crater. While slightly deeper, between 0.3 and 0.6 km asl, the southern branch is the site of D-CLVD and strike slip events on sub vertical faults with diverse directions. The association of normal fault and strike-slip events must be induced by a common stress field existing during the preparation of the two eruptions preceding the April distal eruption.

Fig. 6B shows 17 clusters that cover the 15 days prior to the March eruption. In the southern part of the summit, 10 clusters show strike-slip faulting, with similar orientation, which take place in the southern branch mentioned above, forming a dense seismic zone around 0.5 km asl. In the same locus, five clusters were identified as D-CLVDs. The last

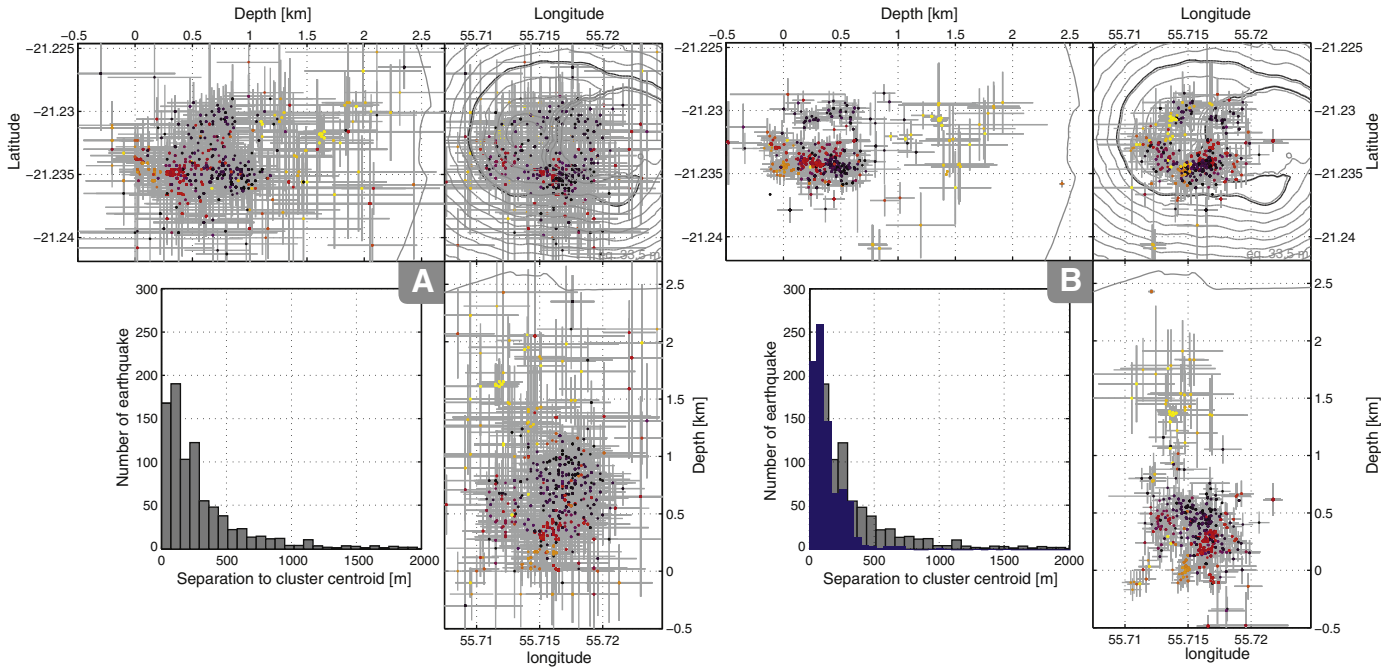

Fig. 4. Comparison between locations and relocation. A : locations from analyst-defined picks ; B : relocation in LSQR mode from correlation catalog. Axis corresponds to geographic coordinates. Both A and B show results obtained with the same set of hand-picked earthquakes, but B also shows automatically picked earthquakes added by cross-correlation clustering. The colors are consistent with Fig. 3A. In the lower left corners, histograms show the distances distribution from cluster centroid to clustered earthquakes.

cluster of March was identified as C-CLVD and was relocated at 0.3 km asl. The association of strike-slip and D-CLVD events below the southern part of the summit is the distinguishing characteristic of the March eruption precursors.

From March 31st to April 5th, before the collapse of Dolomieu crater on April 5th, at 20:50, the summit of PdF shows a clear seismic signature. Fig. 6C shows the short lifetime clusters of Fig. 3A that preceded the collapse of Dolomieu crater. This seismic activity has been relocated under the southern part of the summit, between 0.8 km asl and sea level. Taking into account the location and the phase polarities, 24 clusters of C-CLVDs show a compression axis inclined 80° toward the south-west. In the same time span, we found 7 clusters determined as normal faulting events relocated in the same area as the March strike-slip events, around 0.3 asl. The source determination of all normal mechanism clusters gives the same nodal planes with a north–south strike and a west dip. Observation of the results suggests that normal faulting is linked to the CLVD generator. The comparison of Fig. 6B with Fig. 6C indicates that the strike-slip fault and the D-CLVD of February and March give ways to the C-CLVD clusters before the collapse. From April 1st to April 2nd, earthquakes also occurred at −2 km under the eastern flank of PdF and seemed to be a result of to the return to an equilibrium state of the eastern flank during the final injection toward the eruption locus.

In Fig. 7D, two yellow clusters span the April 5th–June 5th time period and are located under the southern part of the summit, between 0.3 to 0 km, in the same zone as the former CLVD generator and strike-slip area. They show normal faulting with the same orientation of the one observed just before the collapse. Normal faulting also takes place at sea level (purple clusters) with east–west oriented faults. A dense cluster of undeterminable earthquakes has been relocated under the south-western part of Bory crater, around sea level. A fourth cluster denser than the preceding one, starts at −0.5 km, between Bory and Dolomieu craters. Hypocenters of this cluster cannot be constrained to pure double couple or CLVD. An aseismic zone between 0 and 0.5 km bsl could be defined in cross section and the three clusters just described are distributed around this zone. Finally, an U-shaped ring of superficial normal faults underlines the Bory crater, from 1 km asl to 1.5 km asl.

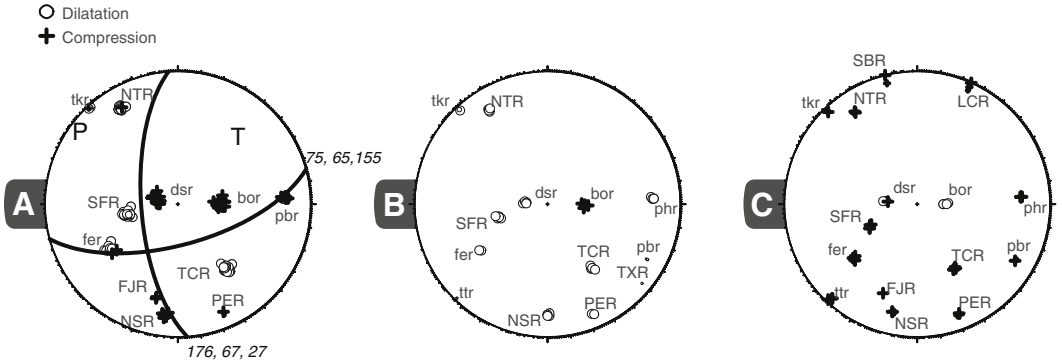

Fig. 5. Three examples of *FPFIT* results. Lower hemispheres are represented. A is a strike slip focal mechanism determined from the polarities of a February cluster (master on 12/02/2007 at 01:44 22 s). B is a dilatation CLVD identified from the polarities of a March cluster (master on 17/03/2007 at 07:58 55 s). C is a pre-collapse compression CLVD identified from the polarities of an April cluster (master on 03/04/2007 at 07:22 11 s).

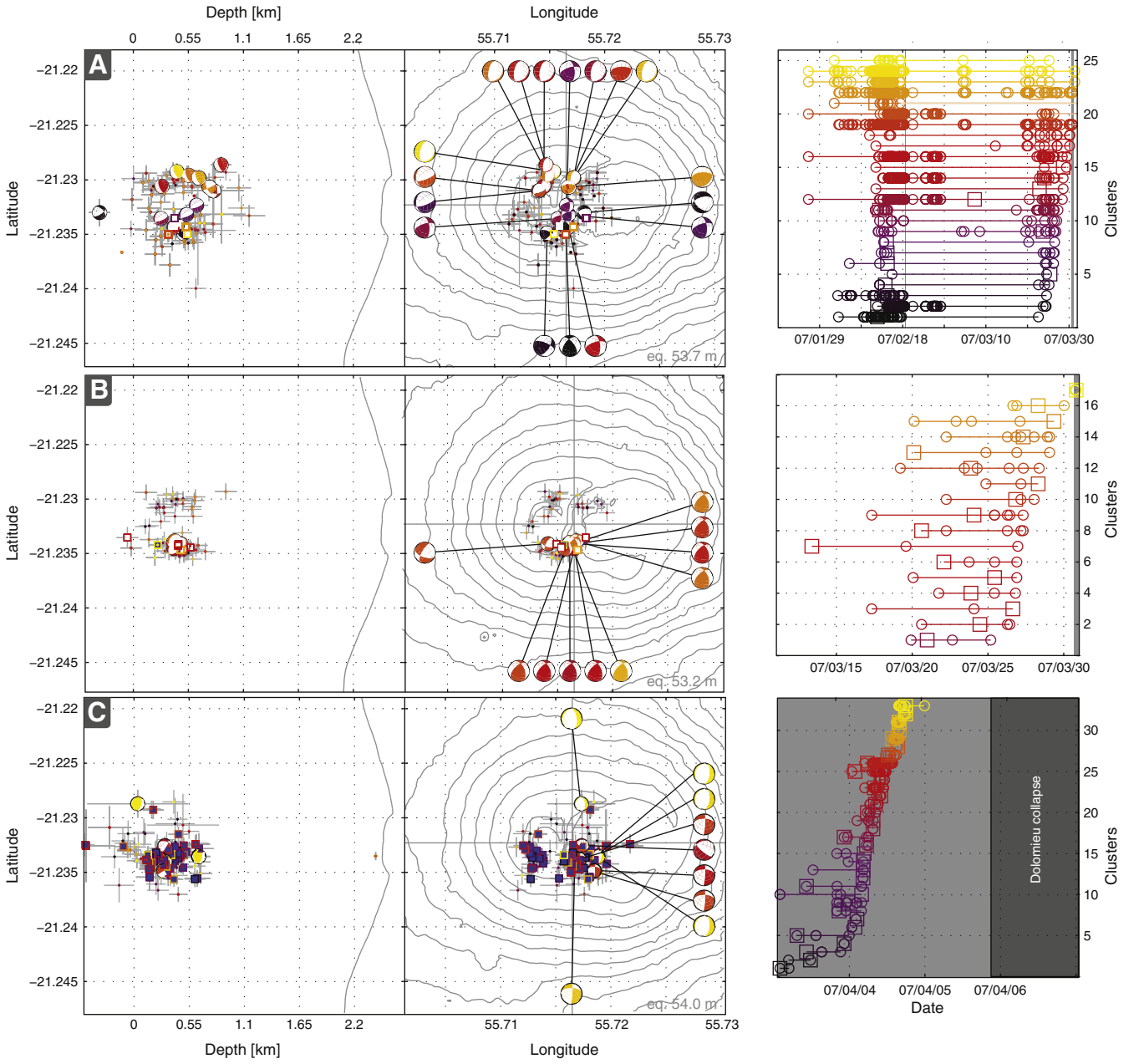

Fig. 6. Seismicity of 2007 eruptions. N–S cross section and map and dendrograms of clusters are plotted from left to right. Beach balls are plotted for each clusters determined as pure double couple, squares are plotted for each cluster with CLVD polarities (dilatation in white, compression in blue). The relocations results are displayed by dots and gray error bars. A: pre-eruptive seismicity occurring both before February and March eruption. B: pre-eruptive seismicity associated only with the preparation of the March 30th proximal eruption. C: seismicity preceding the April 5 collapse.

5.3. Co-seismic slips orientation

For 54 relocated double-couple clusters, we noticed that the distribution of the relocated hypocenters spread over one of the nodal planes, which was chosen to define the fault plane. We then extracted the slip orientation along this plane, considering the motion of the upper block. Their representation provides a general view of the stress field before the collapse of the Dolomieu crater from February to March 31st. Fig. 8 shows co-seismic slips in the northern parts directed towards the center of the volcano while, in the southern parts, the co-seismic slips are oriented outward from the center of the volcano. Cross sections also show two different kinds of slips. In the south-eastern part, co-seismic slips dip 20° above the horizontal, while in the three other parts, co-seismic slips dip 60° below the horizontal. A north–south cross section shows that at 0.8 km a small part of the centripetal and centrifugal slips are mixed in the transition between north and south.

The co-seismic slip in the south-eastern part are extracted from the strike-slip events described before and indicate the existence of an uprising source below the southern part of the summit. The growth of this source started in February (and is responsible for strike-slip events belonging to the clusters common to February and March, Fig. 6A, Section 5.2). This stress field perturbation evolves at the end of March and leads to the aligned strike-slip events of the March cluster, Fig. 6B, Section 5.2. In the northern part, the slip angle of 60° may correspond to a sub-vertical maximum compressive stress, suggesting the force of gravity. To summarize, co-seismic slips show only one stress field perturbation below the southern part of the summit which leads to the up-rising of the south-eastern side toward the S-SE and to the

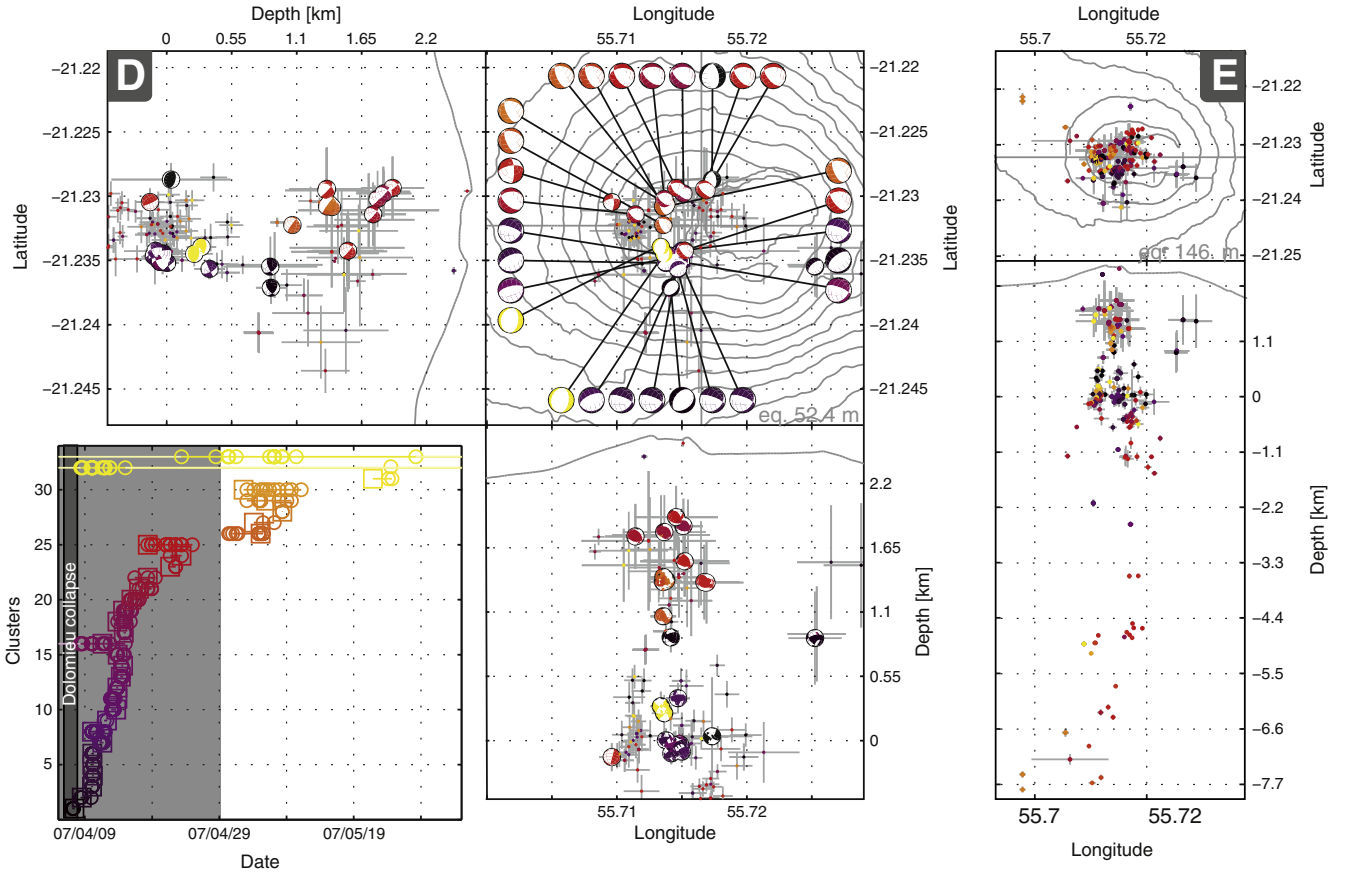

Fig. 7. Post-collapse seismicity. N–S cross section and map and dendrograms of clusters are plotted from left to right. Beach balls are plotted for each clusters determined as pure double couple, squares are plotted for each cluster with CLVD polarities (dilatation in white, compression in blue). The relocation results are displayed by dots and gray error bars. D: the post-collapse seismicity, shallow part, major part of the clustered earthquakes. E : deep part, most of the events below −0.5 km are not clustered. Note that scales of D and E are different.

subsidence of the northern quarters. This perturbation was initiated in February and developed until the end of March.

6. Discussion

Fig. 9 represents the scheme suggested by our results. The initial state of Fig. 9 is composed of a magma chamber located around sea level and a north south radial fault from sea level to 0.8 km, above the southern part of the magma chamber. The tomography of Nercessian et al. (1996) and deformation models of Peltier et al. (2005, 2007, 2009) lead to the hypothesis of a shallow magma chamber feeding the eruptions of PdF localized below the Dolomieu crater, around sea level. Our results show an aseismic zone from −0.5 km to 0 km, slightly shifted toward the west of the Dolomieu crater. Above the magma chamber, we recognized strike slip mechanisms along a network of north–south radial faults. Such radial faults have been highlighted by the structural study of the summit cracks by Bachèlery (1981). Radial cracks are found in the southern and northern part of the summit. All around the two summit craters, Bachèlery (1981) describes several networks of concentric faults. The seismogenic radial faults observed in our study could be linked with the radial cracks in the southern part of the summit. These radial faults are the preferential planes of rupture, and were created before the 2007 eruptions.

6.1. Strike-slip mechanisms

Our clustering results highlight the role of the strike-slip mechanisms which are associated with the preparation of the February and March eruptions. They form a network of radial faults rising from sea level to 0.8 km asl and show oblique focal mechanisms with an uprising component toward the south east. This kind of radial fault may have accommodated the pre-eruptive inflation of the magma chamber with strike-slip motion (Fig. 9B) which opened a vertical volume along the asperity of the radial fault. The opened conduit could be filled by feeding the February and March eruptions. The inflation of a sea level magma chamber before the March eruption has been studied by Peltier et al. (2009) and Augier (2008). The deformation of the February and March eruptions (Peltier, 2007) clearly show a relative uplift of the southern part of the summit, which agrees with the relocation of our oblique strike-slip mechanisms. Furthermore, the intrusion of magma along the radial fault may trigger strike-slip faulting as suggested by the Coulomb stress change calculations by Roman (2005). At Miyakejima volcano, during the 2000 eruption, strike-slip mechanisms associated with the volcano-radial compression axis were also recognized to be associated to lateral intrusion (Uhira et al., 2005). Considering our results and previous studies, the strike-slip column could be the locus of seismic accommodation of the magma chamber inflation, and a preferential path of intrusion. The occurrence of the same strike-slip faults during February and then during March clearly shows that both dyke intrusions started from the same structure and origin.

6.2. The sill hypothesis

The long-lived strike-slip clusters occur with normal faulting clusters. The strike-slip faults could be associated with intrusions, but the normal faults must be interpreted with another phenomenon. The normal faults form a second column, from sea level to 0.8 km above the northern part of the sea level magma chamber. The uplift of the southern part of the magma chamber's roof toward the south east is associated with the subsidence of the northern part of the roof. Such subsidence

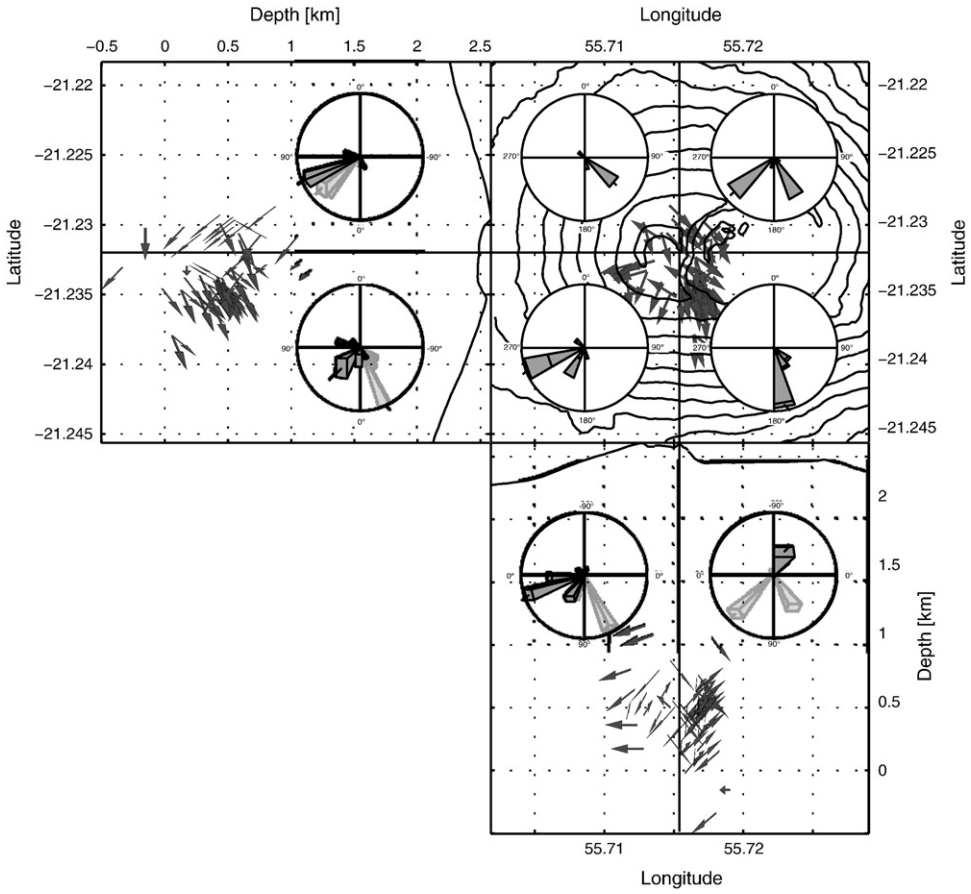

Fig. 8. Measurements of 54 co-seismic slip orientation before Dolomieu crater collapse. The mapped area is divided in four quarters and four rose diagrams. Light gray diagram in E–W cross section corresponds to northern quarters, and in N–S cross section, corresponds to eastern quarters. Gray arrows : co-seismic slip orientation. Contour intervals : 50 m.

does not appear in the specific clusters during the preparation of the March eruption, and is not associated with the magma intrusions in the strike-slip column. We suggest that the normal faulting induced a major phenomenon that started in February: the intrusion of asill from the southern part of the magma chamber toward the April 2nd eruption site. This assumption has not been highlighted by previous studies. GPS displacements (Peltier et al., 2009) and radar interferometry (Augier, 2008) have both highlighted the March 30th intrusion but did not constrained the intrusion toward the April 2nd eruption site. In fact, the deformation data are recorded preferentially around the summit and are influenced by superficial structure, and the amplitudes of the deformations around the central cone of PdF are not easily interpretable. The deformation data cannot disprove the sill hypothesis and the stress field extracted from co-seismic slip orientations is consistent with this idea. We do not expect to constrain the path or velocity of the distal intrusion with seismicity but we show that a detailed study of summit seismicity is helpful for the characterization of a distal intrusion. Also, the work of Taisne et al. (2010) on radiated seismic energy during seismic swarm should lead to great improvements of intrusion models at PdF.

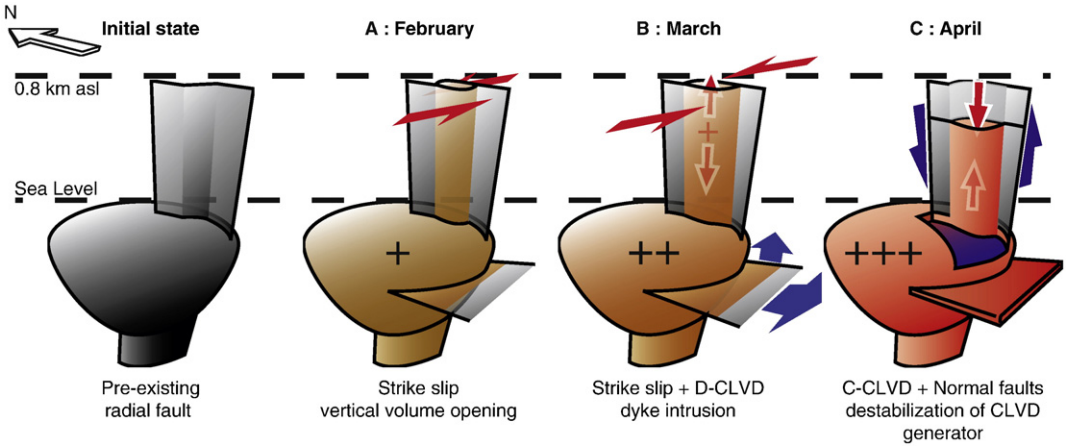

Fig. 9. Structural evolution and the associated magma transfer. Scheme of the structural evolution and the associated magma transfer during the 2007 eruptions at PdF suggested by seismicity. A : preparation of February eruption. B : preparation of March eruption. C : April 2 eruption and Dolomieu collapse source mechanism. See text for details.

6.3. Strike-slip mechanisms and D-CLVD

The strike-slip column is the locus, in March, of D-CLVD activity (Fig. 9B). CLVD mechanisms have been repeatedly observed in volcanic areas and have been interpreted from theory as the result of fluid injection (Aki, 1984; Julian and Sipkin, 1985; Chouet and Julian, 1985; Kanamori et al., 1993). Following Hirn et al. (1991) and according to the column shape of the relocations and its association to sub-vertical post-collapse normal faulting, we assume that the D-CLVDs of March are due to rapid volume increase in vertical fluid filled cracks. Regarding the very similar relocation of strike slip and D-CLVD mechanisms, we propose that there is a link between the strike-slip mechanisms and the D-CLVDs of March. The filling of the radial fault asperities during the inflation of the underlying magma chamber lead to the pressurization of the magma funnel, building a D-CLVD generator which fed the February and March eruptions. Considering the dimensions of the D-CLVD column as a cylinder (800 m high and 75 m in diameter), we obtain an approximate volume of 2.6×10^6 m^3 for the magma funnel area. We cannot distinguish between this volume and the volume associated with the March eruption. Each D-CLVD indicates a step of rapid pressurization of the D-CLVD generator which grew throughout the month of March.

6.4. The C-CLVD crisis

The CLVD generator reached a critical state when, from April 1st to 5th, an intense seismic crisis dominated by C-CLVD mechanisms was recorded (Fig. 9C). We identified 315 earthquakes as C-CLVD from April 1st to 5th. They take place along a column rising from sea level to 0.8 km asl, just above an aseismic zone surrounded by several undeterminable clusters from sea level to −0.5 km. Our study is limited by the lack of tensor inversion which could constrain the volumetric component of CLVD. Possible research about this subject would be complicated by the heterogeneity of the volcanoes physical properties. In fact, at very short periods, especially at small hypocentral distances, the influence of lateral heterogeneity is critical: a 1D model is a very bad approximation of the real medium and is not accurate enough to provide a good agreement between observed and synthetic seismograms. Getting a 3D velocity model on the basis of Greens function computation or extracted from seismic noise interferometry results could provide important improvement. We assume that each C-CLVD from April 1st to April 5th is due to a rapid volume decrease in a vertical fluid filled crack. At this moment, the CLVD generators might be too developed to resist the lithostatic loading during the draining of the underlying magma chamber which started on April 2nd. The chronology of the C-CLVD clusters suggests that C-CLVDs are precursors to the Dolomieu collapse. The waveform clusters of this crisis are very intense and their lifetimes are very short suggesting a network of CLVD sources activated one after the other. The stress field must have been perturbed by a fast structural evolution during the crisis that triggered the Dolomieu collapse.

6.5. The shallow magma chamber and its link to depth

Relocation and source determination results support the existence of a shallow magma chamber and constrain its roof at sea level. For that, three observations of our results are considered: (i) the existence of an aseismic zone between 0 and −0.5 km, (ii) above this zone, the post-collapse normal faulting column and the collapse of the CLVD generator being the most intense seismogenic area in the volcano, (iii) below, a seismic source migration from −0.5 to −8 km, from April 12th to May 8th. We propose that the draining off of the magma chamber between sea level and −0.5 km results in the collapse of vertical fluid filled cracks. When the collapse reached the surface, and during the crumbling of the collapsed fluid filled cracks, the magma chamber suddenly de-pressurized. Finally, the de-pressurization front propagates from the sea level magma chamber toward depth, along a narrow path. The vertical conduit from depth to the sea level magma chamber has been proposed by Pinel and Jaupart (2003) and imaged by Battaglia et al. (2005) from −5 km. Recently Prôno et al. (2009) interpreted their passive tomographic model of PdF by the presence of a magma chamber around −1 km and suggests a network of magma pockets in an intrusive complex from sea level to 1 km. These authors disagree with Nercessian et al. (1996) and propose the existence of a seismic interface at sea level without a sea level magma chamber. Above sea level, this model is in agreement with the first model of the PdF plumbing system proposed by Lénat and Bachèlery (1990) and could be consistent with our results. But we cannot fit our model with the tomographic image of Prôno et al. (2009) of a magma chamber around −1 km. An open conduit shall make the link between the sea level chamber and the 1.2 km bsl chamber.

7. Conclusion

Our results show that the pre-eruptive seismicity of the April 2007 distal eruption of PdF volcano reactivated several clusters that were also active before other distal eruptions of the 2000–2006 period. There is no direct reference in the literature about this subject. For the first time, our results clearly highlight similarities in the seismicity from preparation of eruptions during 2000, 2002, 2004, 2005 and 2007 (Fig. 3B). We do not show here the sources relocations and determinations of clustered earthquakes of 2008 and between 2000 and 2006. This seismicity should be investigated to obtain information about the common seismicity preceding each type of eruption. Future research about this subject will help the monitoring of eruption types at PdF volcano. This study highlights the long lifetime cluster of strike-slip faults, associated with the growing of CLVD generators. The CLVD generators grow during the intrusions supplying the summit and proximal eruptions and have a structure consistent with the stress field induced by the preparation of distal intrusions. Finally, it reached an unstable state in April 2007, and became the source of the caldera collapse and of the opening of the bellowing magma storage level.

Acknowledgements

We are grateful to the staff of the Piton de La Fournaise Volcanological Observatory, for their help in providing seismic data. Thanks to J.M. Farrell, L. Michon, G. Roult and A. Peltier for improvements in the english of this paper. We also thank M. Zhizhin for helpful comments. This is IPGP contribution 3130.

References

Aki, K., 1984. Evidence for magma intrusion during the Mammoth Lakes earthquakes of May 1980 and implication of the absence of volcanic (Harmonic) Tremor. Journal of Geophysical Research 89 (B9), 7689–7696.

Augier, A., 2008. Caractérisation des déplacements liés à l'éruption d'avril 2007 du Piton de la Fournaise (Réunion), analyse à partir de données d'interférométrie radar et modélisation., Master's thesis, Université de Clermont-Ferrand II, ENS Cachan, Clermont-Ferrand, France.

Bachèlery, P., 1981. Le Piton de la Fournaise (île de la Réunion) étude volcanologique, structurale et pétrologique., Ph.D. thesis, Université de Clermont-Ferrand II, Clermont-Ferrand, France.

Battaglia, J., Ferrazzini, V., Staudacher, T., Aki, K., Cheminée, J., 2005. Pre-eruptive migration of earthquakes at the Piton de la Fournaise volcano (Réunion Island). Geophysical Journal International 161 (2), 549–558.

Carter, A., van Wyk de Vries, B., Kelfoun, K., Bachèlery, P., Briole, P., 2007. Pits, rifts and slumps: the summit structure of Piton de la Fournaise. Bulletin of Volcanology 69 (7), 741–756.

Chouet, B., Julian, B.R., 1985. Dynamics of an expanding fluid-filled crack. Journal of Geophysical Research 90 (B13), 11,187–11,198.

Clarke, D., Townend, J., Savage, M., Bannister, S., 2009. Seismicity in the Rotorua and Kawerau geothermal systems, Taupo Volcanic Zone, New Zealand, based on improved velocity models and cross-correlation measurements. Journal of Volcanology and Geothermal Research 180, 50–66.

Courtillot, V., Besse, J., Vandamme, D., Jaegger, J., Montigny, R., 1986. Deccan trap volcanism as a cause of biologic extinctions at the Cretaceous–Tertiary boundary ? Comptes Rendus de l'Académie des Sciences 303 (II), 863–868.

Dvorak, J., 1992. Mechanism of explosive eruptions of Kilauea volcano, Hawaii. Bulletin of Volcanology 54, 638–645.

Fedotov, S., Chirkov, A., Gusev, N., Kovalev, G., Slezin, Y., 1980. The large fissure eruption in the region of Plosky Tobachik volcano in Kamchatka, 1975–1976. Bulletin of Volcanology 43, 47–60.
Filson, J., Simkin, T., Leu, L., 1973. Seismicity of caldera collapse : Galapagos Island, 1968. Journal of Geophysical Research 78, 8591–8621. doi:10.1029/JB078i035p08591.
Fremont, M.-J., Malone, S.D., 1987. High Precision Location of Earthquakes at Mount St Helens, Washington. Journal of Geophysical Research 92 (B10), 10223–10236.
Geshi, N., Shimano, T., Chiba, T., Nakada, S., 2002. Caldera collapse during the 2000 eruption of Miyakejima Volcano, Japan. Bulletin of Volcanology 64 (1), 55–68.
Got, J.-L., Fréchet, J., Klein, F.W., 1994. Deep fault plane geometry inferred from multiplet relative relocation beneath the south flank of Kilauea. Journal of Geophysical Research 99 (B8), 15375–15386.
Hildreth, W., Fierstein, J., 2000. Katmai volcanic cluster and the great eruption of 1912. Geological Society of America Bulletin 112 (10), 1594–1620. doi:10.1130/0016-7606(2000) 112.
Hirn, A., Lépine, J., Sapin, M., Delorme, H., 1991. Episodes of pit-crater collapse documented by seismology at Piton de la Fournaise. Journal of Volcanology and Geothermal Research 47 (1–2), 89–104.
Johnson, C., 1995. Earthworm: a flexible approach to seismic network processing. IRIS Newsletters 14 (2), 1–4.
Julian, B.R., Sipkin, S.A., 1985. Earthquake processes in the Long Valley Caldera area, California. Journal of Geophysical Research 90 (B13), 11,155–11,169.
Kanamori, H., Ekstrom, G., Dziewonski, A., Barker, J.S., Sipkin, S.A., 1993. Seismic radiation by magma injection: an anomalous seismic event near Tori Shima, Japan. Journal of Geophysical Research 98 (B4), 6511–6522.
Kikuchi, M., Yamanaka, K., Kokestu, K., 2001. Source process of the long-period Seismic pulses associated with the 2000 eruption of Miyake-jima volcano, and its implications. Journal of Geography 110 (2), 204–216.
Knopoff, L., Randall, M.J., 1970. The compensated linear-vector dipole: a possible mechanism for deep earthquakes. Journal of Geophysical Research 75 (26), 4957–4963.
Kumagai, H., Ohminato, T., Nakano, M., Ooi, M., Kubo, A., Inoue, H., Oikawa, J., 2001. Very-long-period seismic signals and caldera formation at Miyake Island, Japan. Science 293 (5530), 687–690.
Lee, W., Lahr, J., 1975. Hypo 71 (revised): a computer program for determining hypocenter, magnitude and first motion pattern of local earthquakes. Open file report. U.S. Geological Survey, Menlo Park, Calif.
Lénat, J., Bachèlery, P., 1990. Structure and dynamics of the central zone of Piton de la Fournaise volcano, in Le Volcanisme de la Réunion. In: Lénat, J.-F. (Ed.), Le volcanisme de la Réunion — Monographie: Centre de Recherche en Volcanologie. Clermont-Ferrand, France, pp. 257–296.
Lenat, J., Bachelery, P., Bonneville, A., Tarits, P., Cheminée, J., Delorme, H., 1989. The December 4th 1983 to February 18th 1984 eruption of Piton de la Fournaise volcano (Réunion Island, Indian Ocean): description and interpretation. Journal of Volcanology and Geothermal Research 36, 87–112.
Massin, F., 2009. Transferts et Stockages Magmatiques au Piton de la Fournaise, Ph.D. thesis, Université de la Réunion, St Denis, France.
Michon, L., Staudacher, T., Ferrazzini, V., Bachèlery, P., Marti, J., 2007. The April 2007 collapse of Piton de la Fournaise: a new example of caldera formation. Geophysical Research Letters 34. doi:10.1029/2007GL031248.
Nercessian, A., Him, A., Lépine, J.-C., Sapin, M., 1996. Internal structure of Piton de la Foumaise volcano from seismic wave propagation and earthquake distribution. Journal of Volcanology and Geothermal Research 70 (3–4), 123–143. doi:10.1016/0377-0273(95)00042-9.
Paige, C., Saunders, M., 1982. LSQR: sparse linear equations and least squares problems. Transaction on Mathematical Software 8 (2), 195–209.
Peltier, A., 2007. Suivi, modélisation et évolution des processus d'injections magmatiques au Piton de La Fournaise (Réunion), Ph.D. thesis, Université de La Réunion, Institut de Physique du Globe de Paris, St Denis, France.
Peltier, A., Ferrazzini, V., Staudacher, T., Bachèlery, P., 2005. Imaging the dynamics of dyke propagation prior to the 2000–2003 flank eruptions at Piton de La Fournaise, Réunion Island. Geophysical Research Letters 32 (L22302). doi:10.1029/2005GL023720.
Peltier, A., Staudacher, T., Bachèlery, P., 2007. Constraints on magma transfers and structures involved in the 2003 activity at Piton de La Fournaise from displacement data. Journal of Geophysical Research 112 (B03207). doi:10.1029/2006JB004379.
Peltier, A., Famin, V., Bachèlery, P., Cayol, V., Fukushima, Y., Staudacher, T., 2008. Cyclic magma storages and transfers at Piton de La Fournaise volcano (La Réunion hotspot) inferred from deformation and geochemical data. Earth and Planetary Science Letters 270 (3–4), 180–188. doi:10.1016/j.epsl.2008.02.042.
Peltier, A., Staudacher, T., Bachèlery, P., Cayol, V., 2009. Formation of the April 2007 caldera collapse at Piton de La Fournaise volcano: Insights from GPS data. Journal of Volcanology and Geothermal Research 184, 152–163. doi:10.1016/j.jvolgeores.2008.09.009.
Peltier, A., Bachèlery, P., Staudacher, T., 2009. Magma transport and storage at Piton de La Fournaise (La Réunion) between 1972 and 2007: a review of geophysical and geochemical data. Journal of Volcanology and Geothermal Research 184, 93–108. doi:10.1016/j.jvolgeores.2008.12.008.
Pinel, V., Jaupart, C., 2003. Magma chamber behavior beneath a volcanic edifice. Journal of Volcanology and Geothermal Research 108 (B2), 2072. doi:10.1029/2002JB001751.
Prôno, E., Battaglia, J., Monteiller, V., Got, J.-L., Ferrazzini, V., 2009. P-wave velocity structure of Piton de la Fournaise volcano deduced from seismic data recorded between 1996 and 1999. Journal of Volcanology and Geothermal Research 184 (1–2), 49–62.
Reasenberg, P., Oppenheimer, D., 1985. FPFIT, FPPLOT, and FPPAGE: FORTRAN computer programs for calculating and displaying earthquake fault-plane solutions. U.S. Geological Survey open-file report 85–739. U.S. Dept. of the Interior, Geological Survey.
Roman, D.C., 2005. Numerical models of volcanotectonic earthquake triggering on non-ideally oriented faults. Geophysical Research Letters 32 (L02), 304. doi:10.1029/2004GL021549.
Rowe, C., Thurber, C., White, R., 2004. Dome growth behavior at Soufriere Hills Volcano, Montserrat, revealed by relocation of volcanic event swarms, 1995–1996. Journal of Volcanology and Geothermal Research 134, 199–221. doi:10.1016/j.jvolgeores.2004.01.008.
Saint-Ange, F., 2009. La sédimentation volcanoclastique en contexte de point chaud (île de La Réunion, Océan Indien), Ph.D. thesis, Université de La Réunion, Saint Denis.
Simkin, T., Howard, K.A., 1970. Caldera collapse in the Galápagos Islands, 1968: The largest known collapse since 1912 followed a flank eruption and explosive volcanism within the caldera. Science 169, 429–437.
Staudacher, T., Ferrazzini, V., Peltier, A., Kowalski, P., Boissier, P., Catherine, P., Lauret, F., Massin, F., 2009. The April 2007 eruption and the Dolomieu crater collapse, two major events at Piton de la Fournaise (La Réunion Island, Indian Ocean). Journal of Volcanology and Geothermal Research 184, 126–137. doi:10.1016/j.jvolgeores.2008.11.005.
Taisne, B., Shapiro, N., Brenguier, F., Ferrazzini, V., Albino, F., Pinel, V., 2010. Toward real-time monitoring of dyke propagation from shallow low-amplitude seismicity at Piton de la Fournaise volcano. Geophysical Research Abstracts 12 EGU2010-12808-1.
Uhira, K., Baba, T., Mori, H., Katayama, H., Hamada, N., 2005. Earthquake swarms preceding the 2000 eruption of Miyakejima volcano, Japan. Bulletin of Volcanology 67, 219–230. doi:10.1007/s00445-004-0405-3.
Urai, M., Geshi, N., Staudacher, T., 2007. Size and volume evaluation of the caldera collapse on Piton de la Fournaise volcano during the April 2007 eruption using ASTER stereo imagery. Geophysical Research Letters 34 (L 22318).
Waldhauser, F., Ellsworth, W., 2000. A double-difference earthquake location algorithm: method and application to the Northern Hayward Fault, California. Bulletin of the Seismological Society of America 90 (6), 1353–1368.